Received: 24 October 2018 | Revised: 5 December 2018 | Accepted: 14 December 2018
DOI: 10.1002/ardp.201800309

FULL PAPER

DPhG ARCH PHARM
Archiv der Pharmazie

Potent and highly selective dual-targeting monoamine oxidase-B inhibitors: Fluorinated chalcones of morpholine versus imidazole

Bijo Mathew[1] | Seung C. Baek[2] | Della G. Thomas Parambi[3] | Jae P. Lee[2] | Githa E. Mathew[4] | Sivaraman Jayanthi[5] | Vinod Devaraji[5] | Clariya Rapheal[1] | Devikrishna Vinod[1] | Shahin Shad Kondarath[1] | Md. S. Uddin[6] | Hoon Kim[2]

[1] Division of Drug Design and Medicinal Chemistry Research Lab, Department of Pharmaceutical Chemistry, Ahalia School of Pharmacy, Palakkad, India

[2] Department of Pharmacy and Research Institute of Life Pharmaceutical Sciences, Sunchon National University, Suncheon, Republic of Korea

[3] Department of Pharmaceutical Chemistry, Jouf University, Sakaka, Saudi Arabia

[4] Department of Pharmacology, Grace College of Pharmacy, Palakkad, India

[5] Computational Drug Design Lab, School of Bio Sciences and Technology, Vellore Institute of Technology, Vellore, India

[6] Department of Pharmacy, Southeast University, Dhaka, Bangladesh

Correspondence
Bijo Mathew, Division of Drug Design and Medicinal Chemistry Research Lab, Department of Pharmaceutical Chemistry, Ahalia School of Pharmacy, Palakkad-678557, Kerala, India.
Email: bijovilaventgu@gmail.com

Hoon Kim, Department of Pharmacy and Research Institute of Life Pharmaceutical Sciences, Sunchon National University, Suncheon 57922, Republic of Korea.
Email: hoon@sunchon.ac.kr

Funding information
Basic Science Research Program through the National Research Foundation (NRF) of Korea, which is funded by the Ministry of Education, Grant number: 2017R1D1A3B03028559

Abstract

Two series of fluorinated chalcones containing morpholine and imidazole-based compounds (**f1–f8**) were synthesized and evaluated for recombinant human monoamine oxidase (MAO)-A and -B as well as acetylcholinesterase inhibitory activities. Our results indicate that morpholine containing chalcones are highly selective MAO-B inhibitors having reversibility properties. All the imidazole-based fluorinated chalcones showed weak MAO inhibitions in both isoforms. Among the tested compounds, (2*E*)-3-(3-fluorophenyl)-1-[4-(morpholin-4-yl)phenyl]prop-2-en-1-one (**f2**) showed potent inhibitory activity for recombinant human MAO-B (IC_{50} = 0.087 μM) with a high selectivity index (SI) of 517.2. In the recovery experiments using dialysis, the residual activity of MAO-B inhibited by **f2** was close to that with the reversible reference inhibitor. Inhibition assays revealed that the K_i values of **f1** and **f2** for MAO-B were 0.027 and 0.020 μM, respectively, with competitive patterns. All the morpholine-based compounds (**f1**–**f4**) showed moderate inhibition toward acetylcholinesterase with IC_{50} values ranging between 24 and 54 μM. All morpholine-containing compounds exhibit good blood–brain barrier permeation in the PAMPA method. The rational approach regarding the highly selective MAO-B inhibitor **f2** was further ascertained by induced fit docking and molecular dynamics simulation studies.

KEYWORDS
acetylcholinesterase, chalcone, entrance cavity, imidazole, MAO-B selective inhibitor, molecular dynamics, morpholine

Bijo Mathew and Seung C. Baek contributed equally to this work.

1 | INTRODUCTION

Parkinson's disease (PD) encompasses a multicentric progressive loss of specific neuronal cell populations resulting in the development of the movement disorder. PD is the second most prevalent age-related neurodegenerative disease that results from the loss of nigrostriatal dopaminergic neurons.[1] The neurodegeneration is initiated decades before it affects the motor function, and the phenotype is usually characterized by resting tremors, rigidity, and bradykinesia.[2] Monoamine oxidase (MAO; EC 1.4.3.4) has increased expression levels in neuronal tissues as well as gastro and hepatic tissues.[3] MAO-A and MAO-B inhibitors are in clinical use for the treatment of neurological and psychiatric disorders, respectively.[4] Biochemically, these two isoenzymes are differentiated by their substrate and inhibitor specificities.[5] Inhibition of isoform B, which is mainly localized in the raphe nucleus of serotonergic neuronal cell bodies, leads to elevated levels of dopamine (DA) in Parkinsonism patients. The phenomenal advances in neurochemistry have greatly helped in unfolding the pathophysiology of this disorder and provided the basis for the introduction of levodopa. The new understanding and disclosure of the mechanisms of 1-methyl-4-phenyl-1,2,5,6-tetrahydropyridine (MPTP) in primate models has triggered a resurgence concerning the etiological factors that enhance the inhibition of MAO-B with deprenyl, the first MAO-B inhibitor which potentiates the effects of levodopa and prolongs the life of PD patients.[6]

Most MAO-B inhibitors are devoid of the "cheese effect," a property that attributes these drugs as exciting prospects for further investigation as neurodegenerative disease therapeutics.[7] Based on their kinetics of inhibition, there are two classes of MAO-B inhibitors: reversible and irreversible.[8] Reversible inhibitors are usually structurally similar to MAO substrates and actively bind to the site but are metabolized slower. Irreversible or suicide inhibitors first bind in a reversible competitive manner and are then oxidized by a FAD cofactor, which then makes it unavailable for amine metabolism.[9] Usually, the MAO-B inhibitors are designed to elevate the reduced DA concentrations responsible for PD, wherein at least 80% of the enzyme needs to be inhibited to achieve pharmacological action.[10]

Alzheimer's disease (AD) is another common neurodegenerative disease characterized by dementia, behavioral disturbances, and difficulties in daily living activities.[11] The deficiency in cholinergic neurotransmission results in memory and cognitive deficits in AD patients. Inhibition of acetylcholinesterase (AChE), which catalyzes the degradation of acetylcholine, improves the cholinergic function, and is a target which represents an innovative therapeutic weapon for the treatment of AD.[12] Studies reveal that selective MAO-B inhibitors such as selegiline, rasagiline, and safinamide retard the further neurodegeneration and have a positive effect on memory modalities in AD.[13] Recent *in vivo* studies in mice reported the correlation between the progress of AD and MAO activity.[14] Based on the drug design concept of "one molecule, multiple-targets,"[15] we aim to synthesize a multi-target chalcone-based molecular frame work possessing inhibitory potential to both MAO-B and AChE. Chalcone motifs are extensively recognized by many groups addressing the discovery of novel selective MAO-B and AChE inhibitors.[16–20] Furthermore, dual and multi-targeted approaches toward MAO-B and AChE inhibitions for the development of potential therapeutic agents for AD and PD have recently been reported.[21]

Chalcone chemistry is a fascinating area in the field of medicinal chemistry due to its wide target-based mechanism, easy synthesis, and structural versatility.[22] Chemically, it consists of two aryl or heteroaryl rings separated by an α–β unsaturated carbonyl linker; ring **A** is nearer to the carbonyl system and ring **B** is nearer to the β-carbon of the unsaturated unit[23] (Figure 1). Numerous structural manipulations in chalcone motifs have been endeavored to develop highly selective reversible MAO inhibitors. These efforts are mainly focused for the development of MAO-B inhibitors rather than MAO-A.[24] It has largely been reported that the presence of electron donating or lipophilic groups such as methyl, dimethylamino, ethyl, bromine, fluorine, and trifluoromethyl groups at ring **B** of chalcones are favorable for MAO-B inhibitory activity.[25–29] Simultaneously, the effect of heterocyclic systems such as thiophene, indole, furan, and imidazole in ring **A** also produced promising MAO-B inhibitory potencies by maintaining the above-mentioned pharmacophore on ring **B**.[30–40] These two structural manipulations have resulted in the development of a diverse class of MAO-B inhibitors encompassing competitive mode of inhibition. The current study focuses on the effect of the morpholine and imidazole heterocyclic systems at the *para* position of the ring **A** of phenyl system and the fine tuning of fluorine on the phenyl ring **B** in the chalcones. Our group has previously reported a new class of fluorinated chalcones as hMAO-B inhibitors (Figure 2). Accordingly, the current study describes the synthesis of morpholine/imidazole-based fluorinated chalcones, and investigates their potential for MAO inhibition, kinetics, reversibility mode, and blood–brain barrier (BBB) permeation property. In addition, AChE inhibitory actions are also investigated. Finally, we identify the lead molecule from the *in vitro* results of MAO-B inhibitor by performing a detailed molecular dynamics simulation.

2 | RESULTS AND DISCUSSION

2.1 | Chemistry

The synthesis of fluorinated heteroaryl chalcones was accomplished by Claisen–Schmidt condensation between

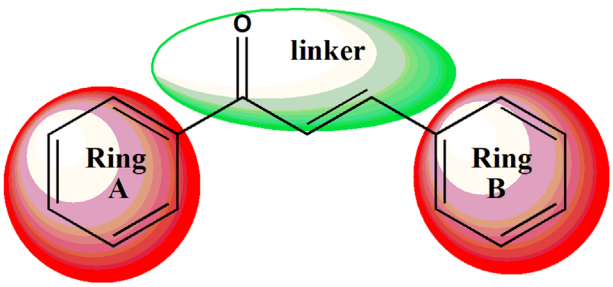

FIGURE 1 Chalcone motif

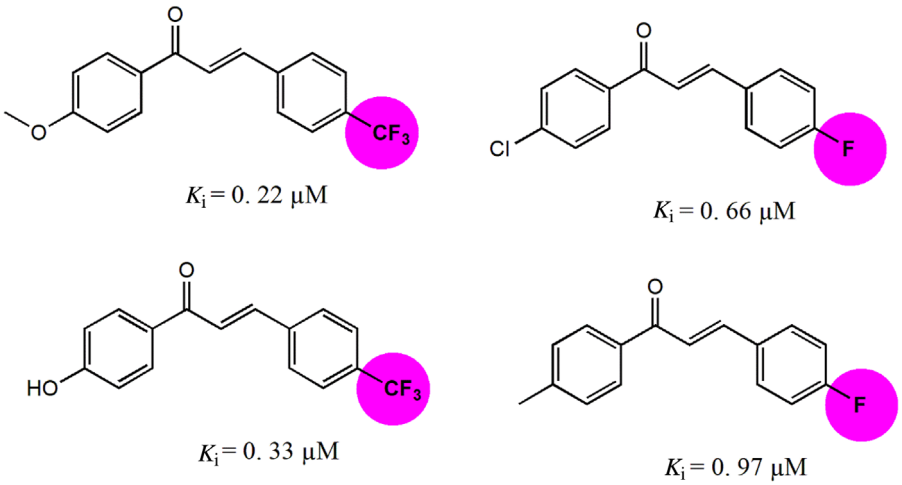

FIGURE 2 Potent fluorinated chalcones as MAO-B inhibitors reported by our group[26–28]

morpholine/imidazole-based heteroaryl methyl ketones and various fluorinated benzaldehydes in the presence of an alkaline alcoholic medium (Scheme 1). The ^{1}H NMR spectra of **f1**–**f4** showed that H_1 and H_2 protons of the morpholine ring resonated at 3.33–3.36 and 3.84–3.88 ppm as triplets, respectively. H_α and H_β protons of fluorinated heteroaryl chalcones appeared as sharp doublets at 7.33–7.58 and 7.68–8.15 ppm, respectively. The large coupling constant (*J*) of these doublets (16 Hz) confirmed the *trans* configuration of the chalcones. Mass spectra of all fluorinated chalcones showed intensive molecular ions, secondary to the structure of the targeted compounds.

2.2 | Biology

2.2.1 | MAO inhibition studies

The preliminary investigation suggests that morpholine containing fluorinated chalcone compounds are highly selective hMAO-B inhibitors as compared to imidazole (Table 1). The study mainly focuses on (i) the effect of morpholine and imidazole heterocyclic system at the *para* position of ring **A** of the chalcones and (ii) effect and orientation of the fluorine unit at **B** ring. All the imidazole-based fluorinated chalcones showed lesser MAO inhibition in both isoforms, except **f8** (hMAO-B IC_{50} = 9.07 μM), which was previously reported along with **f7**.[40] Two of the most active compounds from these series were morpholine-containing compounds **f1** and **f2** with IC_{50} values of 0.14 and 0.087 μM, respectively, against hMAO-B. These compounds differed in the position of the fluorine atom on ring **B** of the chalcone core. It is noticeable that shifting of fluorine to *ortho* and *para* positions of ring **B** of chalcones decreases the MAO-B inhibitory potency when compared to *meta* substitution. This fluorine orientation pattern has no impact on imidazole-based chalcones. This suggests a clear structure–activity relation principle that the fluorine orientation pattern in morpholine containing compounds renders effectiveness against hMAO-B inhibition.

In morpholine containing compounds, shifting of fluorine to *para* (**f3**) decreased the potency toward hMAO-B (IC_{50} = 0.21 μM).

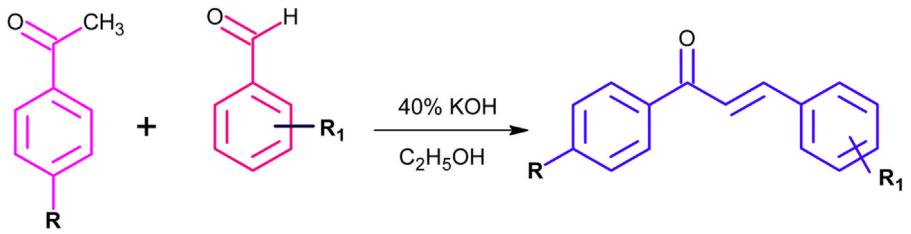

R	R_1	R	R_1
f1: Morpholine	-2F	**f5**: Imidazole	-2F
f2: Morpholine	-3F	**f6**: Imidazole	-3F
f3: Morpholine	-4F	**f7**: Imidazole	-4F
f4: Morpholine	-4CF_3	**f8**: Imidazole	-4CF_3

SCHEME 1 Synthesis of fluorinated chalcones

TABLE 1 Inhibition of MAO-A, MAO-B, and AChE by fluorinated heteroaryl chalcones[a]

	Residual activity at 10 μM (%)			IC_{50} (μM)			
Compounds	MAO-A	MAO-B	AChE	MAO-A	MAO-B	AChE	SI[b]
f1	62.0 ± 1.4	−2.6 ± 0.1	84.4 ± 0.39	18.69 ± 0.34	0.14 ± 0.005	48.06 ± 0.55	133.5
f2	78.5 ± 0.7	−3.4 ± 0.4	80.1 ± 0.27	45.0 ± 2.84	0.087 ± 0.008	>50.0	517.2
f3	88.5 ± 2.1	1.06 ± 1.4	80.5 ± 0.05	>50.0	0.21 ± 0.006	>50.0	>47.6
f4	87.5 ± 2.1	34.0 ± 5.7	77.0 ± 0.96	>50.0	2.30 ± 0.20	24.52 ± 0.27	>4.3
f5	87.5 ± 0.7	78.3 ± 7.1	93.9 ± 0.42	>50.0	>10.0	>50.0	
f6	84.0 ± 2.8	59.4 ± 5.7	95.8 ± 0.67	>50.0	>10.0	>50.0	
f7	80.5 ± 2.1	69.2 ± 7.1	95.4 ± 0.32	>50.0	>10.0	>50.0	
f8	84.0 ± 1.4	42.5 ± 7.8	98.0 ± 0.75	>50.0	9.07 ± 0.52	>50.0	>1.1
Toloxatone				0.96 ± 0.036	–		
Lazabemide				–	0.032 ± 0.0056		
Clorgyline				0.0046 ± 0.0002	>2.0		
Pargyline				>2.0	0.097 ± 0.0047		
Tacrine						0.24 ± 0.015	

[a]Results are expressed as means ± SD of duplicate experiments. The value for tacrine was obtained after 15 min pre-incubation with enzyme.
[b]SI values for MAO-B were obtained by dividing IC_{50} values of MAO-A by those of MAO-B.

Replacing fluorine with trifluoromethyl group at the same position (**f4**) also resulted in decreased inhibition (IC_{50} = 2.30 μM). Interestingly, **f2** showed an extremely high selectivity index (SI) for MAO-B (517.2), suggesting that **f2** is a highly selective inhibitor for MAO-B. The potency of **f2** for MAO-B (K_i = 0.020) was higher than the synthesized furanochalcone derivatives (K_i > 0.072 μM), except for one compound (2*E*,4*E*)-1-(furan-2-yl)-5-phenylpenta-2,4-dien-1-one (**F1**) (K_i = 0.0041 μM) previously reported by our group.[39] However, the SI value of **f2** (517.2) in this study was three times higher than that of the lead furanochalone (**F1**) of the previous study (172.4).[39] However, although the potency (IC_{50} = 0.087 μM) of **f2** for MAO-B was 2.7 times lower than the marketed drug for MAO-B lazabemide (IC_{50} = 0.032 μM), the values were within a comparable range in nanomolar concentration. The potency of **f2** (0.087 μM) was also more than to the standard hMAO-B irreversible type inhibitor pargyline (0.097 μM) (Table 1). Furthermore, our studies revealed that the **f2** molecule has some structural similarity with the FDA approved selective hMAO-A inhibitor moclobemide (Figure 3). The morpholine containing tail, electron rich linker and halogenated phenyl head are common structural features of both motifs, which may contribute to the similarity in targeting MAO.

2.2.2 | AChEe inhibition

As seen in Table 1, all compounds are less potent than the reference compound tacrine for AChE inhibition. However, the morpholine-based compounds (**f1–f4**) showed moderate inhibition toward AChE, with IC_{50} values ranging between 24 and 54 μM, based on the reported classification.[41] The data showed that the imidazole nucleus may not be a crucial factor for the inhibitory potency against AChE in fluorinated chalcones. Effect of fluorine orientation also shows moderate inhibition in morpholine containing compounds for AChE

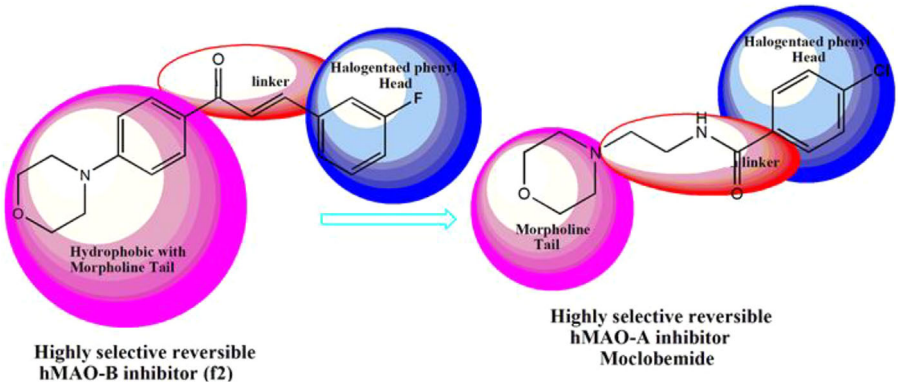

FIGURE 3 Similar structural features of **f2** and moclobemide

inhibition. The *ortho*- and *para*-substituted analogues **f1** and **f3** show slightly higher AChE inhibition compared to the *meta*-substituted analogue **f3**, unlike observed for MAO-B inhibition. Interestingly, the presence of trifluoromethyl group at the *para* position of ring **B** of morpholine chalcones shows two times higher potency than the fluorinated compounds.

2.2.3 | Kinetics

The inhibition modes of **f1** and **f2** for MAO-B were analyzed by Lineweaver–Burk plots. Plots for both **f1** and **f2** were linear intersecting the *y*-axis (Figure 4A and C). The secondary plot of slopes versus inhibitor concentrations provided the K_i values of **f1** and **f2** for MAO-B inhibitions, determined to be 0.027 ± 0.002 and 0.020 ± 0.002 μM, respectively (Figure 4B and D). These results indicate that **f1** and **f2** are selective and reversible competitive inhibitors of MAO-B. Comparing the inhibition constants, the inhibition constant of **f2** was much lower than the irreversible reference hMAO-B inhibitor selegiline (0.14 μM), as previously reported by our research group.[32–36]

Reversibility studies

No changes in activity were observed for **f2** with MAO-B up to 30 min of preincubation, suggesting the interaction between MAO-B and **f2** was nearly instantaneous. In reversibility experiments, A_D and A_U values obtained for **f2** were 70.1% and 26.7%, respectively (Figure 5). For the reference experiments, A_D and A_U values for lazabemide were 73.4% and 35.0%, and for pargyline were 28.5% and 27.5%, respectively. After dialysis, inhibition by pargyline remained constant. However, inhibition by lazabemide was greatly recovered, similar to the inhibition by **f2**. These results indicate that **f2** is a reversible inhibitor of MAO-B.

2.3 | BBB prediction

The parallel artificial membrane permeation assay (PAMPA) is used to determine the BBB permeation potential of a compound. According to the limits established by Di et al.,[42] BBB permeation test compounds are classified as follows:

$$\text{CNS+ (high BBB permeation predicted)}: Pe\left(\times 10^{-6}\ \text{cms}^{-1}\right) > 4.00$$

$$\text{CNS− (low BBB permeation predicted)}: Pe\left(\times 10^{-6}\ \text{cms}^{-1}\right) < 2.00$$

Table 2 indicates the permeability of commercial drugs obtained by PAMPA-BBB assay and the top ranked four morpholine containing

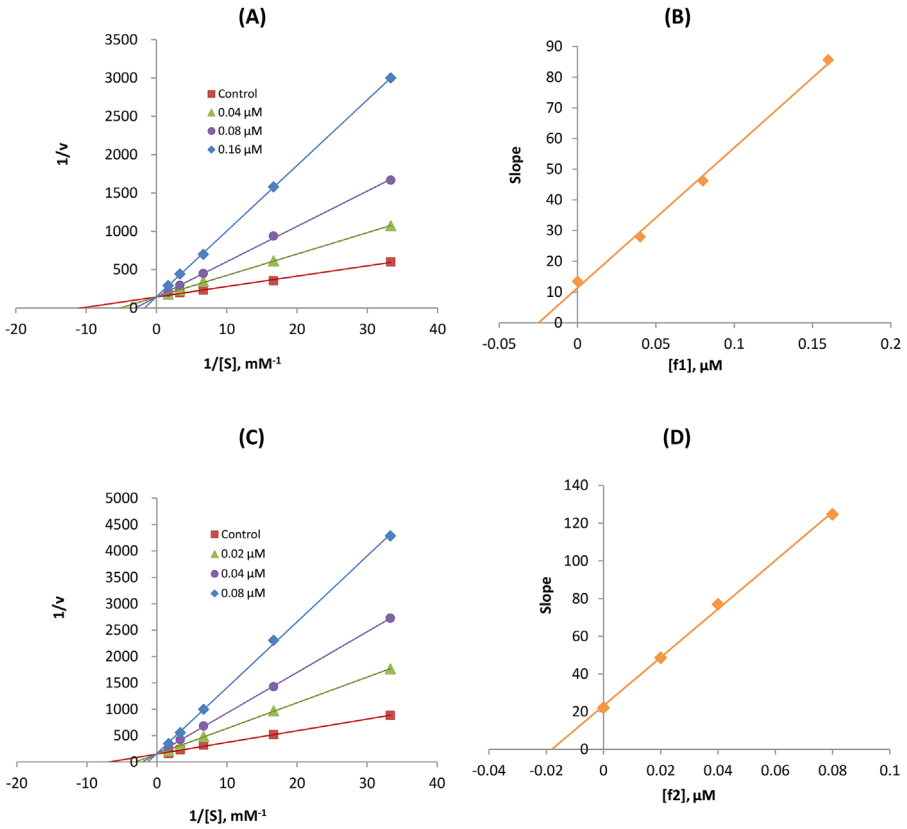

FIGURE 4 Lineweaver–Burk plots for inhibition of MAO-B by **f1** (A) and **f2** (C), and their respective secondary plots of slopes versus inhibitor concentrations for **f1** (B) and **f2** (D)

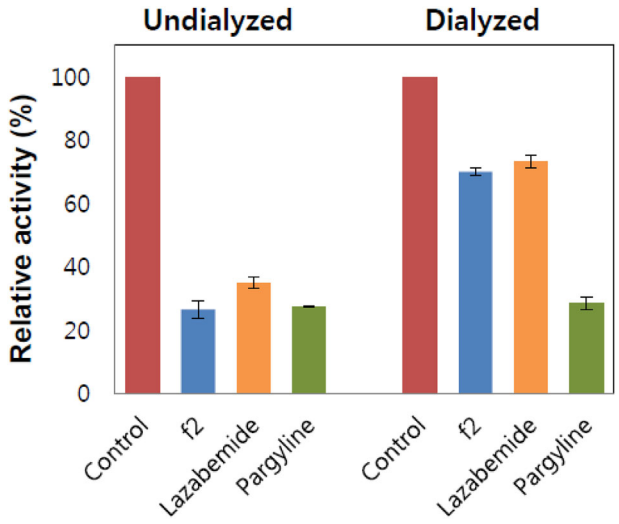

FIGURE 5 Reversibility mode of **f2**

fluorinated chalcones. The results show that all the tested chalcones can efficiently cross the BBB to target the MAO-A and MAO-B enzymes in the central nervous system (CNS), which is consistent with our design strategy. All the morpholine containing chalcones show higher permeability than the standard testosterones. We particularly highlight that the highest permeability value achieved of **f4** in the series may be due to the presence of a lipophilic trifluoromethyl group.

2.4 | Computational studies

2.4.1 | Molecular docking and dynamics

Docking software performance was validated by calculating the crystal pose RMSD (root mean square deviation) in place against the pose generated by the Glide software for ligands. When two crystal protein PDBs such as 2V61 (ligand id C18) and 2V5Z (ligand id HRM) were used, RMSD values were 0.862 and 1.121 by Glide XP docking (Figure 6). Therefore, we used same settings for this study.

The compound, (2*E*)-3-(3-fluorophenyl)-1-[4-(morpholin-4-yl)-phenyl]prop-2-en-1-one (**f2**) was docked against MAO-B (2V61) to generate least energy with best pose. Results indicate that it holds π–π interactions with Tyr326 and Tyr398 surrounded by hydrophobic pocket environment Ile326, Trp119, Pro104, Phe103, Leu164, Leu167, Ile199, Cys172, Tyr188, Tyr326, Leu328, Tyr60, and Tyr435. The fluorinated **A** ring of morpholine chalcone was directed toward the FAD unit within close proximity of the N5 atom (Figure 6). Polar residue Gln206 collectively gives the protein-ligand complex total energy of −20834 kcal/mol, docking score of −11.520, and contains ligand Epik penalty which gives a glide XP score of −10.381 and subsequently an IFD score of −20941.70, which are good affinity scores for ligand binding. Stable protein-ligand pose are subjected to explicit molecular dynamics to check the stability, interactions, and consistency of protein ligand complex for 50 ns time period. As per RMSD (root mean square deviations) analysis, the protein C-alpha and ligand were stable in the range 1.7–2.2 Å for a long duration of simulation time without any major fluctuations; we therefore conclude that the complexes were energetically compatible (Figure 7). The interaction patterns were strongly observed with π–π interactions with Tyr326 and other hydrophobic networks, H-bonds with amino acids such as His90, Phe99, Pro104, Trp119, Leu167, Phe168, Leu171, Cys172, Ile198, Ile199, Ile316, and Tyr326, and H bonds with Thr201, Gln205, Gln206, Tyr206, Tyr326, Phe343, Tyr398, and Tyr435. Major water bridges between the protein and ligand formed were Ile199, Ser200, Thr201, Gly205, Gly206, Thr316, Tyr326, and Phe343, whereas minor bridges were with formed Gln65, Tyr60, Gly101, and Cys172 (Figures 8 and 9). The overall impression of the ligand–protein interaction analysis and C-alpha protein and ligand RMSD plots and nonbonding interactions indicate that **f2** is reasonably stable in the MAO-B protein, and we hypothesize that **f2** is an active molecule with major Tyr326 π–π and hydrophobic interaction that could be the critical cause evoking the biological response.

3 | CONCLUSION

The study mainly corroborated the MAO and AChE inhibitory effect of morpholine and imidazole heterocyclic nucleus on the *para* position of ring **A** of fluorinated chalcones. Fine tuning of the fluorine atom on the

TABLE 2 PAMPA-BBB of morpholine-based fluorinated chalcones and commercial drugs

Compounds[a]	Bibliography *Pe* ($\times 10^{-6}$ cms^{-1})[b]	Experimental *Pe* ($\times 10^{-6}$ cms^{-1})[c]	Prediction
f1	–	18.31 ± 0.24	CNS+
f2	–	18.14 ± 0.26	CNS+
f3	–	18.58 ± 0.65	CNS+
f4	–	19.43 ± 0.45	CNS+
Testosterone	17.0	17.33 ± 0.12	CNS+
Progesterone	9.3	08.13 ± 0.42	CNS+
Dopamine	0.2	0.21 ± 0.01	CNS−
Hydrocortisone	1.8	1.71 ± 0.02	CNS−

[a]Compounds were dissolved in DMSO (5 mg/mL) and diluted to be 100 μg/mL with PBS/EtOH (70:30).
[b]Taken from Ref. [42].
[c]Values were shown as the mean ± SEM of three independent experiments.

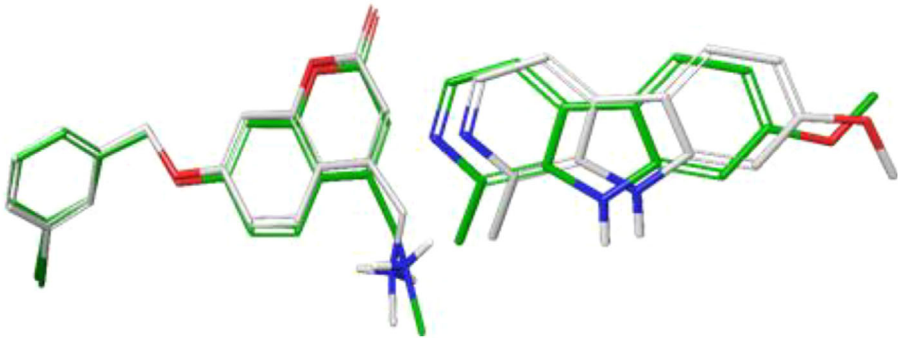

FIGURE 6 Docking validation-crystal ligand pose (gray) versus docked pose (green) for 2V61 and 2V5Z

various positions of ring **B** of chalcones markedly alters the activity. The results document that morpholine bearing fluorinated chalcones are potent and highly selective hMAO-B inhibitors with moderate AChE inhibition. All the imidazole-based fluorinated chalcones showed weak MAO inhibitions in both isoforms. We further postulate that **f2** is a potential candidate as a multi-targeting compound, being a potent and selective MAO-B inhibitor (0.087 μM) and moderate AChE inhibitor (53.41 μM). The K_i values of potent molecules **f1** and **f2** for MAO-B were 0.027 and 0.020 μM, respectively, and showed competitive inhibitions. Percentage of the relative activity of **f2** on dialyzed and undialyzed values is 70.1 and 26.7%, respectively, indicating the formation of a reversible hMAO-B-inhibitor complex.

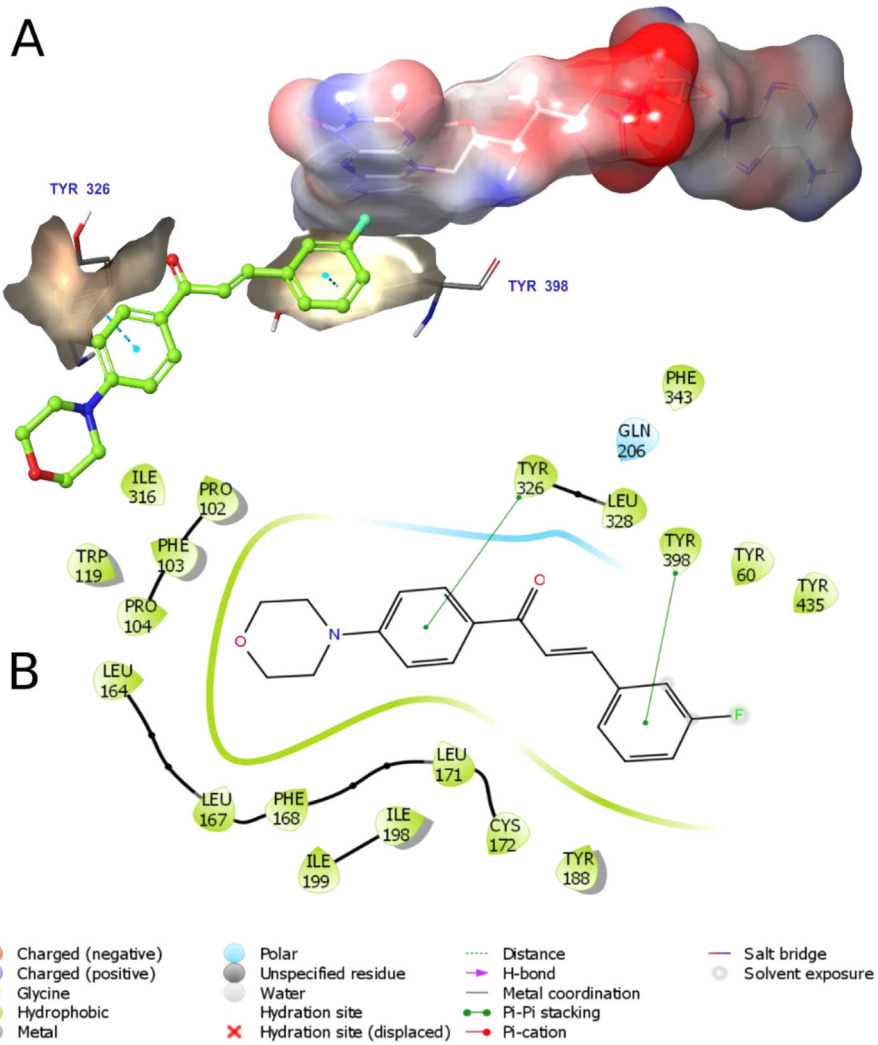

FIGURE 7 Induced fit best pose of **f2** for 3D-dimensional (ligand in ball and stick and interacting residues with molecular surface with FAD cofactor) (A) and 2D-interaction image (B) against MAO-B

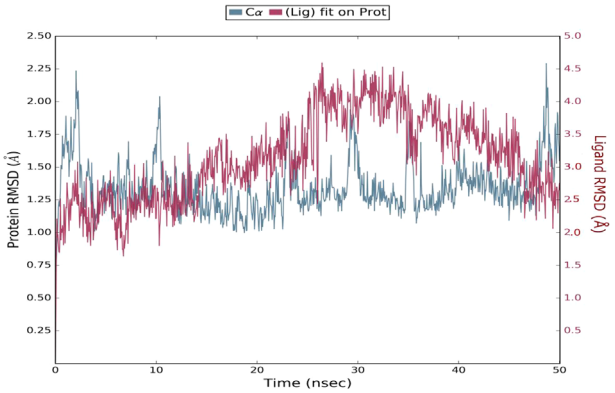

FIGURE 8 Protein-ligand RMSD

The BBB permeation assay method strongly indicates that all the morpholine containing fluorinated chalcones have the ability to cross the BBB which is a consistent requirement for the development of multi-targeted MAO-B inhibitors for various neurodegenerative disorders. Computational studies revealed that morpholine bearing phenyl ring of **f2** exhibits a π–π stacking interaction with Tyr326. Highly selective inhibition of hMAO-B with moderate inhibition with AChE of **f2** shows the potential therapeutic application of this compound for the treatment of AD and PD.

4 | EXPERIMENTAL

4.1 | Chemistry

4.1.1 | Synthesis

Equimolar quantities of substituted fluorinated benzaldehyde and 4′-morpholinoacetophenone or 4′-imidazoleacetophenone were dissolved in 40% KOH. The reaction mixture was stirred for 12 h and was poured into ice-cold water. The precipitated product was washed using water, dried, and recrystallized from methanol.

The original spectra of the investigated compounds are provided as Supporting Information, as are their InChI codes together with some biological activity data.

(2*E*)-3-(2-Fluorophenyl)-1-[4-(morpholin-4-yl)phenyl]prop-2-en-1-one (f1)

Yellow, m.p. 118–120°C. ^{1}H NMR (400 MHz, $CDCl_3$) δ: 3.35–3.34 (4H, t, morpholine -N-$(CH_2)_2$), 3.87–3.86 (4H, t, morpholine O-$(CH_2)_2$), 6.93–6.90 (2H, d,$H_{3'}$ & $H_{5'}$), 6.93–6.84 (2H, d, H_3 & H_5), 7.17–7.10 (2H, m, H_4 & H_6), 7.37–7.33 (1H, d, *J* = 16 Hz, -CH_α), 7.89–7.85 (1H, d, *J* = 16 Hz, -CH_β), 8.03–8.00 (2H, d, $H_{2'}$ & $H_{6'}$). ESI-MS (*m/z*): calculated 311.350, observed 311.349.

(2*E*)-3-(3-Fluorophenyl)-1-[4-(morpholin-4-yl)-phenyl]prop-2-en-1-one (f2)

Yellow, m.p. 116–118°C. ^{1}H NMR (400 MHz, $CDCl_3$) δ: 3.33–3.32 (4H, t, morpholine -N-$(CH_2)_2$), 3.85–3.84 (4H, t, morpholine O-$(CH_2)_2$), 6.90–6.87 (2H, d, $H_{3'}$ & $H_{5'}$), 7.40–7.06 (4H, m, H_2, H_4, H_5 & H_6), 7.56–7.52 (1H, d, *J* = 16 Hz, -CH_α), 7.75–7.71 (1H, d, *J* = 16 Hz, -CH_β), 8.01–7.98 (2H, d, $H_{2'}$ & $H_{6'}$). ESI-MS (*m/z*): calculated 311.350, observed 311.349.

(2*E*)-3-(4-Fluorophenyl)-1-[4-(morpholin-4-yl)phenyl]prop-2-en-1-one (f3)

Pale yellow, m.p. 150–152°C. ^{1}H NMR (400 MHz, $CDCl_3$) δ: 3.35–3.34 (4H, t, morpholine -N-$(CH_2)_2$), 3.88–3.87 (4H, t, morpholine O-$(CH_2)_2$), 6.90–6.87 (2H, d, $H_{3'}$ & $H_{5'}$), 7.12–7.00 (2H, m, H_3 & H_5), 7.50–7.46 (1H, d, *J* = 16 Hz, -CH_α), 7.64–7.61 (2H, m, H_2 & H_6), 7.77–7.73 (1H, d, *J* = 16 Hz, -CH_β), 8.01–7.99 (2H, d, $H_{2'}$ & $H_{6'}$). ESI-MS (*m/z*): calculated 311.350, observed 311.350.

(2*E*)-1-[4-(Morpholin-4-yl)phenyl]-3-[4-(trifluoromethyl)phenyl]-prop-2-en-1-one (f4)

Yellow, m.p. 85–87°C. ^{1}H NMR (400 MHz, $CDCl_3$) δ: 3.36–3.35 (4H, t, *J* = 4 hz, morpholine -N-$(CH_2)_2$), 3.88–3.87 (4H, t, *J* = 8 Hz, morpholine

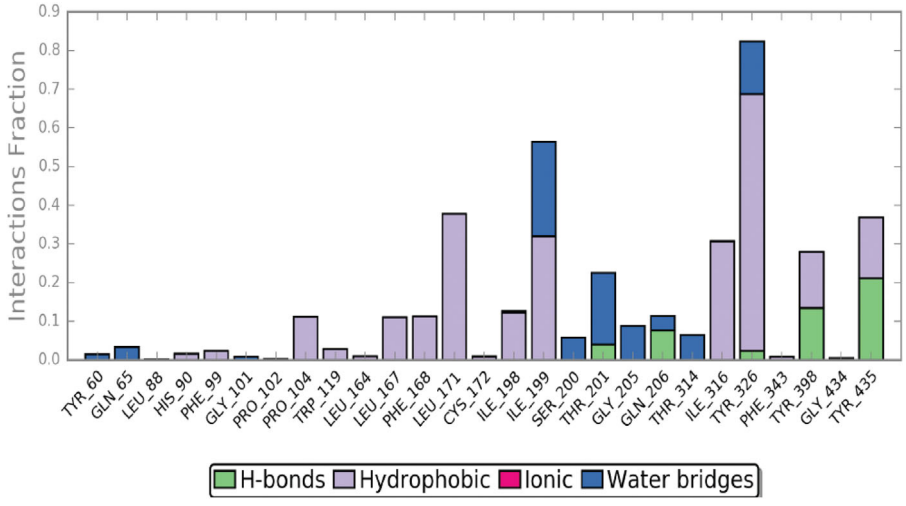

FIGURE 9 Protein interaction fractions with **f2**

O-(CH_2)$_2$), 6.90–6.87 (2H, d, $H_{3'}$ & $H_{5'}$), 7.12–7.00 (2H, m, H_3 & H_5), 7.51–7.47 (1H, d, J = 16 Hz, -CH_α), 7.64–7.61 (2H, m, H_2 & H_6), 7.84–7.80 (1H, d, J = 16 Hz, -CH_β), 8.01–7.99 (2H, d, $H_{2'}$ & $H_{6'}$). ESI-MS (*m/z*): calculated 361.357, observed 361.350.

(2*E*)-3-(2-Fluorophenyl)-1-[4-(1*H*-imidazol-1-yl)phenyl]prop-2-en-1-one (f5)

Orange, m.p. 135–137°C. ^{1}H NMR (400 MHz, $CDCl_3$) δ: 6.93–6.90 (2H, d, $H_{3'}$ & $H_{5'}$), 6.88–6.79 (2H, d, H_3 & H_5), 7.12–7.15 (2H, m, H_4 & H_6), 7.20–7.25 (3H, d, ImH), 7.38–7.33 (1H, d, J = 16 Hz, -CH_α), 8.15–8.11 (1H, d, J = 16 Hz, -CH_β), 8.03–8.00 (2H, d, $H_{2'}$ & $H_{6'}$). ESI-MS (*m/z*): calculated 292.307, observed 292.299.

(2*E*)-3-(3-Fluorophenyl)-1-[4-(1*H*-imidazol-1-yl)phenyl]prop-2-en-1-one (f6)

Pale red, m.p. 148–150°C. ^{1}H NMR (400 MHz, $CDCl_3$) δ: 6.88–6.82 (2H, d, $H_{3'}$ & $H_{5'}$), 7.26–7.21 (3H, d, ImH), 7.40–7.06 (4H, m, H_2, H_4, H_5 & H_6), 7.43–7.39 (1H, d, J = 16 Hz, -CH_α), 7.75–7.71 (1H, d, J = 16 Hz, -CH_β), 8.01–7.98 (2H, d, $H_{2'}$ & $H_{6'}$). ESI-MS (*m/z*): calculated 292.307, observed 292.299.

(2*E*)-3-(4-Fluorophenyl)-1-[4-(1*H*-imidazol-1-yl)phenyl]prop-2-en-1-one (f7)

Brick red, m.p. 140–142°C. ^{1}H NMR (400 MHz, $CDCl_3$) δ: 6.90–6.86 (2H, d, $H_{3'}$ & $H_{5'}$), 7.10–7.02 (2H, m, H_3 & H_5), 7.24–7.20 (3H, d, ImH), 7.46–7.42 (1H, d, J = 16 Hz, -CH_α), 7.68–7.63 (2H, m, H_2 & H_6), 7.79–7.75 (1H, d, J = 16 Hz, -CH_β), 8.03–8.00 (2H, d, $H_{2'}$ & $H_{6'}$). ESI-MS (*m/z*): calculated 292.307, observed 292.299.

(2*E*)-1-[4-(1*H*-Imidazol-1-yl)phenyl]-3-[4-(trifluoromethyl)-phenyl]prop-2-en-1-one (f8)

Saffron red, m.p. 152–154°C. ^{1}H NMR (400 MHz, $CDCl_3$) δ: 6.91–6.88 (2H, d, $H_{3'}$ & $H_{5'}$), 7.14–7.06 (2H, m, H_3 & H_5), 7.25–7.21 (3H, d, ImH), 7.42–7.38 (1H, d, J = 16 Hz, -CH_α), 7.65–7.62 (2H, m, H_2 & H_6), 7.72–7.68 (1H, d, J = 16 Hz, -CH_β), 8.04–8.00 (2H, d, $H_{2'}$ & $H_{6'}$). ESI-MS (*m/z*): calculated 342.314, observed 342.315.

4.2 | Enzyme assays

MAO-A and MAO-B activities were measured by the continuous method using kynuramine (0.06 mM) and benzylamine (0.3 mM) as the substrates as described previously[40] and expressed as changes in absorbance per min. K_m values for kynuramine and benzylamine were 0.035 and 0.15 mM, respectively; the concentrations for both substrates were 1.7× and 2.0 × K_m values, respectively. The chemicals and enzymes used were as described previously.[43] AChE activity was assayed using the method previously described,[44] with slight modifications. The mixture was reacted at 25°C for 10 min with monitoring at 412 nm using AChE (0.2 U/mL) from *Electrophorus electricus* (Type VI-S, Sigma). The mixture contained 0.5 mM of 5,5′-dithiobis(2-nitrobenzoic acid) (DTNB) and 0.5 mM of acetylthiocholine iodide (ACTI) in 0.5 mL of 50 mM sodium phosphate (pH 7.5).

4.2.1 | Analysis of inhibitory activities and kinetics

The inhibitory potential of the eight compounds for MAO-A or MAO-B were primarily analyzed at 10 μM concentrations. Thereafter, we determined the IC_{50} values for compounds possessing greater than 50% inhibitory activity. Reversible and irreversible reference inhibitors were included as standards. The time-dependence of the inhibition by the most potent compound **f2** for MAO-B was further investigated, as previously described.[45] K_i values and inhibition types of the inhibitors were determined by kinetic studies, as described previously.[43] The AChE inhibitory activities by the compounds were measured by pre-incubating for 15 min with the enzyme prior to the measurement.

4.2.2 | Analysis of inhibitor reversibility

The reversibility of the most potent inhibitor **f2** for MAO-B was investigated by the dialysis method using DiaEasy dialyzers (BioVision Inc., Milpitas, CA, USA), as previously described.[45] Concentrations used were ~2 × IC_{50}: 0.18 μM of **f2**, 0.08 μM of lazabemide, and 0.20 μM of pargyline. Residual activities for undialyzed and dialyzed sets were separately measured, after preincubation with MAO-B for 30 min. The relative values for undialyzed (A_U) and dialyzed (A_D) assays were calculated comparing with each control set without inhibitor. The reversibility pattern was concluded by comparing A_U and A_D values with the references.

4.3 | BBB assay

The top-ranked four synthesized morpholine-based fluorinated chalcones and the commercial drugs were dissolved in DMSO to a final concentration of 5 mg/mL. Compounds were then diluted with a mixture of phosphate-buffered saline solution and ethanol (PBS/EtOH, 70:30) to a final concentration of 25 μg/mL. The filter membrane in donor microplate was coated with polar brain lipid (PBL) dissolved in dodecane (4 μg/mL, 20 mg/mL). A total of 200 μL of diluted solution and 300 μL of PBS/EtOH (70:30) were added to the donor and the acceptor wells, respectively. The donor plate was carefully placed on the acceptor plate and the sandwich was kept at 25°C for 16 h. The donor plate was carefully removed, and then the concentrations of the compounds in the acceptor, donor, and reference wells were measured with a UV plate reader.[42]

4.4 | Computational studies

All computational works were performed using Schrodinger suite (Small-Molecule Drug Discovery Suite 2018-2, Schrödinger, LLC, New York, NY, 2018).

4.4.1 | Protein and ligand preparation

The protein (PDB: 2V61) used in the study was prepared using the protein preparation wizard where it was processed for fixing the structural issues arising from X-ray crystallography experimental

limitations such as missing hydrogens, side chains or loops and bond orders concerns.[46] In this process, protein is also completely reviewed and modified to retain water and heteroatoms critical for calculations, followed by optimization of hydrogen bond orientations and restrained minimization. A convergence threshold of 0.30 Å with OPLS 2005 force field was used to generate least energy and a problem free protein system to be used for the computational studies.[47] All the organic ligands used in the manuscripts are prepared by Ligprep and used 3D coordinates using OPLS 2005 to maintain molecule's integrity and stereochemistry, ionization at biological pH with minimized 3D coordinates using OPLS 2005 force field.[48]

4.4.2 | Flexible docking

The bioactive pose of molecules were generated using induced fit docking or receptor flexible docking for highly active molecules using the Schrodinger IFD tool against RCSB PDB ID (MAO-B) 2V61 which was prepared earlier using protein preparation. A force field 2005 extended sampling protocol was set to generate 80 poses with receptor hetero atom as the centroid for grid center. The sample ring conformations, with an energy window 2.5 kcal/mol that penalizes the amide, bonds non-planar conformations, and all loops within 5.0 Å were subjected for loop conformations to explore ligand induced effects in the protein that generates best least energy protein ligand poses.[49,50]

4.4.3 | Molecular dynamics

Explicit molecular dynamics study for active ligand **F2** against MAO-B receptor using the aqueous solvent system was first prepared for the protein-ligand complex using the Desmond system builder panel with TIP4P aqueous solvation. Orthorhombic box shape and size was minimized, followed by ions placements, after which membrane details were added as per Protein Data Bank of Transmembrane proteins (http://pdbtm.enzim.hu/) using force field 2005. The prepared systems were subjected to minimization relaxation molecular dynamics followed by productions runs for 50 ns simulation time with NPT ensemble at 300 K and pressure at 1.01325 bar. The pressure was maintained by the Martyna–Tobias–Klein barostat and temperature was regulated using a Nose-Hoover chain thermostat. Approximately 1000 frames for entire protein-ligand simulations could be used for protein ligand interactions and stability trajectory analysis.[51]

ACKNOWLEDGMENTS

This research was supported by the Basic Science Research Program through the National Research Foundation (NRF) of Korea, which is funded by the Ministry of Education (2017R1D1A3B03028559) (to H. Kim).

CONFLICT OF INTEREST

The authors have declared no conflict of interest.

ORCID

Bijo Mathew http://orcid.org/0000-0002-6658-4497

REFERENCES

[1] C. W. Olanow, W. G. Tatton, *Annu. Rev. Neurosci.* **1999**, *22*, 123.
[2] J. K. Andersen, *Nat. Med.* **2004**, *10*, S18.
[3] R. R. Ramsay, *Curr. Pharm. Des.* **2013**, *19*, 2529.
[4] B. Mathew, G. E. Mathew, J. Suresh, G. Ucar, R. Sasidharan, J. K. Vilapurathu, S. Anbazhagan, V. Jayaprakash, *Curr. Enzyme Inhib.* **2016**, *12*, 115.
[5] M. B. Youdim, D. Edmondson, K. F. Tipton, *Nat. Rev. Neurosci.* **2006**, *7*, 295.
[6] M. B. Youdim, Y. S. Bakhle, *Br. J. Pharmacol.* **2006**, *147*, S287.
[7] J. P. Finberg, M. Tenne, *Br. J. Pharmacol.* **1982**, *77*, 13.
[8] S. Carradori, R. Silvestri, *J. Med. Chem.* **2015**, *58*, 6717.
[9] R. H. Abeles, A. L. Maycock, *Acc. Chem. Res.* **1976**, *9*, 313.
[10] P. Foley, M. Gerlach, M. B. Youdim, P. Riederer, *Parkinsonism Relat. Disord.* **2000**, *6*, 25.
[11] L. N. Zhao, L. Lu, L. W. Chew, Y. Mu, *Int. J. Mol. Sci.* **2014**, *15*, 12631.
[12] I. E. Orhan, F. S. Senol, *Curr. Top. Med. Chem.* **2016**, *16*, 1889.
[13] D. Knez, M. Sova, U. Kosak, S. Gobec, *Fut. Med. Chem.* **2017**, *9*, 811.
[14] D. Kim, S. H. Baik, S. Kang, S. W. Cho, J. Bae, M. Y. Cha, M. J. Sailor, I. M. Jung, K. H. Ahn, *ACS Cent. Sci.* **2016**, *2*, 967.
[15] R. R. Ramsay, M. R. Popovic-Nikolic, M. L. Bolognesi, *Clin. Transl. Med.* **2018**, *7*, 3.
[16] F. Chimenti, R. Fioravanti, A. Bolasco, P. Chimenti, D. Secci, F. Rossi, M. Yanez, F. Orallo, F. Ortuso, S. Alcaro, *J. Med. Chem.* **2009**, *52*, 2818.
[17] A. Hammuda, R. Shalaby, S. Rovida, D. E. Edmondson, C. Binda, A. Khali, *Eur. J. Med. Chem.* **2016**, *114*, 162.
[18] H. R. Liu, X. J. Liu, H. Q. Fan, J. J. Tang, X. H. Gao, W. K. Liu, *Bioorg. Med. Chem.* **2014**, *22*, 6124.
[19] H. R. Liu, C. Zhou, H. Q. Fan, J. J. Tang, L. B. Liu, X. H. Gao, Q. A. Wang, W. K. Liu, *Chem. Biol. Drug Des.* **2015**, *86*, 517.
[20] H. R. Liu, H. Fan, X. Gao, X. Haung, X. Liu, L. Liu, C. Zhou, J. Tang, Q. Wang, W. Liu, *J. Enzyme Inhib. Med. Chem.* **2016**, *31*, 580.
[21] L. Pisani, M. Catto, F. Leonetti, O. Nicolotti, A. Stefanachi, F. Campagna, A. Carotti, *Curr. Med. Chem.* **2011**, *18*, 4568.
[22] B. Mathew, A. A. Adeniyi, M. Joy, G. E. Mathew, A. Pillay, C. Sudarsanakumar, M. E. S. Soliman, *J. Mol. Struct.* **2017**, *1147*, 682.
[23] B. Mathew, J. Suresh, S. Anbazhagan, J. Paulraj, G. K. Krishnan, *BioMed. Prev. Nut.* **2014**, *4*, 451.
[24] B. Mathew, A. Haridas, J. Suresh, G. E. Mathew, G. Ucar, V. Jayaprakash, *Cent. Nerv. Syst. Agents Med. Chem.* **2016**, *16*, 120.
[25] J. W. Choi, B. K. Jang, N. Cho, J. H. Park, S. K. Yeon, E. J. Ju, Y. S. Lee, G. Han, A. N. Pae, D. J. Kim, K. D. Park, *Bioorg. Med. Chem.* **2015**, *23*, 6486.
[26] B. Mathew, G. E. Mathew, G. Uçar, I. Baysal, J. Suresh, J. K. Vilapurathu, A. Prakashan, J. K. Suresh, A. Thomas, *Bioorg. Chem.* **2015**, *62*, 22.
[27] B. Mathew, G. E. Mathew, G. Uçar, I. Baysal, J. Suresh, S. Mathew, A. Haridas, V. Jayaprakash, *Chem. Biodiversity* **2016**, *13*, 1046.
[28] B. Mathew, G. Uçar, G. E. Mathew, S. Mathew, P. K. Purapurath, F. Moolayil, S. Mohan, S. V. Gupta, *ChemMedChem* **2016**, *11*, 2649.
[29] B. Mathew, G. E. Mathew, G. Ucar, M. Joy, E. K. Nafna, K. K. Lohidakshan, J. Suresh, *Int. J. Bio. Macromol.* **2017**, *104*, 1321.
[30] B. Mathew, G. Uçar, S. Yabanoğlu-Çiftçi, I. Baysal, J. Suresh, G. E. Mathew, J. K. Vilapurathu, N. A. Moosa, N. Pullarottil, L. Viswam, A. Haridas, F. Fathima, *Lett. Org. Chem.* **2015**, *12*, 605.

[31] S. Zaib, S. U. F. Rizvi, S. Aslam, M. Ahmad, S. M. A. Abid, M. al-Rashida, *Med. Chem*. **2015**, *11*, 580.
[32] B. Mathew, A. Haridas, G. Uçar, I. Baysal, A. A. Adeniyi, M. E. S. Soliman, *Int. J. Bio. Macromol*. **2016**, *91*, 680.
[33] B. Mathew, A. Haridas, G. Uçar, I. Baysal, M. Joy, G. E. Mathew, B. Lakshmanan, V. Jayaprakash, *ChemMedChem* **2016**, *11*, 1161.
[34] B. Mathew, A. A. Adeniyi, S. Dev, M. Joy, G. Ucar, G. E. Mathew, M. E. Soliman, *J. Phys. Chem. B* **2017**, *121*, 1186.
[35] B. Mathew, G. Ucar, C. Raphael, G. E. Mathew, M. Joy, K. E. Machaba, *ChemistrySelect* **2017**, *2*, 11113.
[36] R. Sasidharan, S. L. Manju, G. Ucar, I. Baysal, B. Mathew, *Arch. Pharm. Chem. Life Sci*. **2016**, *349*, 627.
[37] S. J. Robinson, J. P. Petzer, A. Petzer, J. J. Bergh, A. C. U. Lourens, *Bioorg. Med. Chem. Lett*. **2013**, *23*, 4985.
[38] C. Minders, J. P. Petzer, A. Petzer, A. C. U. Lourens, *Bioorg. Med. Chem. Lett*. **2015**, *25*, 5270.
[39] J. Suresh, S. C. Baek, S. P. Ramakrishnan, H. Kim, B. Mathew, *Int. J. Bio. Macromol*. **2018**, *108*, 660.
[40] R. Sasidharan, S. C. Baek, S. L. Manju, H. Kim, B. Mathew, *Biomed. Pharmacother*. **2018**, *106*, 8.
[41] T. C. dos Santos, T. M. Gomes, B. A. S. Pinto, A. L. Camara, A. M. A. Paes, *Front Pharmacol*. **2018**, *9*, 1192.
[42] L. Di, E. H. Kerns, K. Fan, O. J. McConnell, G. T. Carter, *Eur. J. Med. Chem*. **2003**, *38*, 223.
[43] S. C. Baek, H. W. Lee, H. W. Ryu, M. G. Kang, D. Park, S. H. Kim, M. L. Cho, S. R. Oh, H. Kim, *Bioorg. Med. Chem. Lett*. **2018**, *28*, 584.
[44] G. L. Ellman, K. D. Courtney, V. Jr Andres, R. M. Feather-Stone, *Biochem. Pharmacol*. **1961**, *7*, 88.
[45] H. W. Lee, H. W. Ryu, M. G. Kang, D. Park, S. R. Oh, H. Kim, *Bioorg. Med. Chem. Lett*. **2016**, *26*, 4714.
[46] Schrödinger Release 2018-2: Schrödinger Suite 2018-2 Protein Preparation Wizard; Epik, Schrödinger, LLC, New York, NY, 2016; Impact, Schrödinger, LLC, New York, NY, 2016; Prime, Schrödinger, LLC, New York, NY, 2018.
[47] G. M. Sastry, M. Adzhigirey, T. Day, R. Annabhimoju, W. Sherman, *J. Comput. Aid. Mol. Des*. **2013**, *27*, 221.
[48] Schrödinger Release 2018-2: LigPrep, Schrödinger, LLC, New York, NY, **2018**.
[49] W. Sherman, T. Day, M. P. Jacobson, R. A. Friesner, R. Farid, *J. Med. Chem*. **2006**, *49*, 534.
[50] Schrödinger Release 2018-2: Schrödinger Suite 2018-2 Induced Fit Docking protocol; Glide, Schrödinger, LLC, New York, NY, 2016; Prime, Schrödinger, LLC, New York, NY, 2018.
[51] Schrödinger Release 2018-2: Desmond Molecular Dynamics System, D. E. Shaw Research, New York, NY, 2018. Maestro-Desmond Interoperability Tools, Schrödinger, New York, NY, 2018.

SUPPORTING INFORMATION

Additional supporting information may be found online in the Supporting Information section at the end of the article.

How to cite this article: Mathew B, Baek SC, Thomas Parambi DG, et al. Potent and highly selective dual-targeting monoamine oxidase-B inhibitors: Fluorinated chalcones of morpholine versus imidazole. *Arch Pharm Chem Life Sci*. 2019;1–11. https://doi.org/10.1002/ardp.201800309